5 Set Oriented Numerical Methods in Space Mission Design

MICHAEL DELLNITZ[1] AND OLIVER JUNGE[2]
[1]*Institute for Mathematics, University of Paderborn, Germany*
[2]*Center for Mathematical Sciences, Munich University of Technology, Germany*

Contents

5.1 Introduction

New techniques for the design of energy efficient trajectories for space missions have been proposed which are based on the circular restricted three-body problem as the underlying mathematical model. These techniques exploit the structure and geometry of certain invariant sets and associated invariant manifolds in phase space in order to systematically construct efficient flight paths.

In this chapter we present numerical methods that enable an implementation of this approach. Using a set oriented framework we show how to compute approximations to invariant sets and invariant manifolds and how to detect connecting orbits that might serve as initial guesses for the solution of a more detailed model. We also show how to extend the approach in order to account for a continuously applied control force on the spacecraft as realized by certain low thrust propulsion systems.

All techniques described in this chapter have been implemented within the software package "Global Analysis of Invariant Objects" (GAIO) which is available from the authors.

5.2 Dynamical systems and mission design

A new paradigm for the construction of energy efficient trajectories for spacecraft is currently emerging. It heavily bases on concepts and techniques from the theory and

numerical treatment of dynamical systems. The basic strategy is the following: Instead of a two-body problem, as in more classical approaches, one considers a restricted three-body problem as the mathematical model for the motion of the spacecraft. This enables one to exploit the intricate structure and geometry of certain invariant sets and their stable and unstable manifolds in phase space—which are not present in two-body problems—as candidate regions for energy efficient trajectories. For example, this approach has recently been used in the design of the trajectory for the *Genesis discovery mission*[1] [29].

Building on this basic concept, techniques have been proposed that synthesize partial orbits from different three-body problems into a single one, yielding energy efficient trajectories with eventually very complicated itineraries [26, 27]. In Ref. [27], a *petit grand tour* among the moons of Jupiter has been constructed by this approach. The idea of the technique is as follows: One computes the intersection of parts of the stable resp. unstable manifold of two specific periodic orbits in the vicinity of two moons, respectively, with a suitably chosen surface. After a transformation of these two curves into a common coordinate system one identifies points on them that lie close to each other—ideally one searches for intersection points. Typically, however, these two curves will not intersect in the chosen surface, so a certain (impulsive) maneuver of the spacecraft will be necessary in order to transit from the part of the trajectory on the unstable manifold to the one on the stable manifold. In a final step this "patched 3-body approximation" to a trajectory is used as an initial guess for standard local solvers using the full *n*-body dynamics of the solar system as the underlying model (as, e.g., the differential corrector implemented in the JPL-tool LTool [32]).

5.2.1 The circular restricted three-body problem

Let us briefly recall the basics of the (*planar*) *circular restricted three body problem* (*PCR3BP*)—for a more detailed exposition and a description of the full spatial model see Refs. [2, 31, 38]. The PCR3BP models the motion of a particle of very small mass within the gravitational field of two heavy bodies (e.g., The Sun and The Earth). Those two *primaries* move in a plane counterclockwise on circles about their common center of mass with the same constant angular velocity. One assumes that the third body does not influence the motion of the primaries while it is only influenced by the gravitational forces of the primaries.

In a normalized rotating coordinate system the origin is the center of mass and the two primaries are fixed on the *x*-axis at $(-\mu, 0)$ and $(1-\mu, 0)$, respectively, where $\mu = m_1/(m_1 + m_2)$ and m_1 and m_2 are the masses of the primaries. The equations of motion for the spacecraft with position (x_1, x_2) in rotating coordinates are given by

$$\ddot{x}_1 - 2\dot{x}_2 = \Omega_{x_1}(x_1, x_2), \qquad \ddot{x}_2 + 2\dot{x}_1 = \Omega_{x_2}(x_1, x_2) \tag{5.1}$$

---

[1] http://genesismission.jpl.nasa.gov.

with

$$\Omega(x_1, x_2) = \frac{x_1^2 + x_2^2}{2} + \frac{1 - \mu}{r_1} + \frac{\mu}{r_2} + \frac{\mu(1 - \mu)}{2}$$

and

$$r_1 = \sqrt{(x_1 + \mu)^2 + x_2^2}, \qquad r_2 = \sqrt{(x_1 - 1 + \mu)^2 + x_2^2}.$$

The system posesses five equilibrium points (the *Lagrange points*): the collinear points L_1, L_2 and L_3 on the *x*-axis and the equilateral points L_4 and L_5. The equations (5.1) have a first integral, the *Jacobi integral*, given by

$$C(x_1, x_2, \dot{x}_1, \dot{x}_2) = -(\dot{x}_1^2 + \dot{x}_2^2) + 2\Omega(x_1, x_2). \qquad (5.2)$$

The three-dimensional manifolds of constant *C*-values are invariant under the flow of (5.1), their projection onto position-space, the *Hill's region*, determines the allowed region for the motion of the spacecraft (Figure 5.1(a)).

5.2.2 Patching three-body problems

The idea of constructing energy efficient trajectories via coupling three-body problems essentially relies on two key observations:

1. For suitable energy values (i.e., values of the Jacobi integral (5.2)) there exist periodic solutions, the *Lyapunov orbits* (Figure 5.1(a)), of (5.1) in the vicinity of the equilibrium points L_1 and L_2 that are unstable in both time directions. Their unstable resp. stable
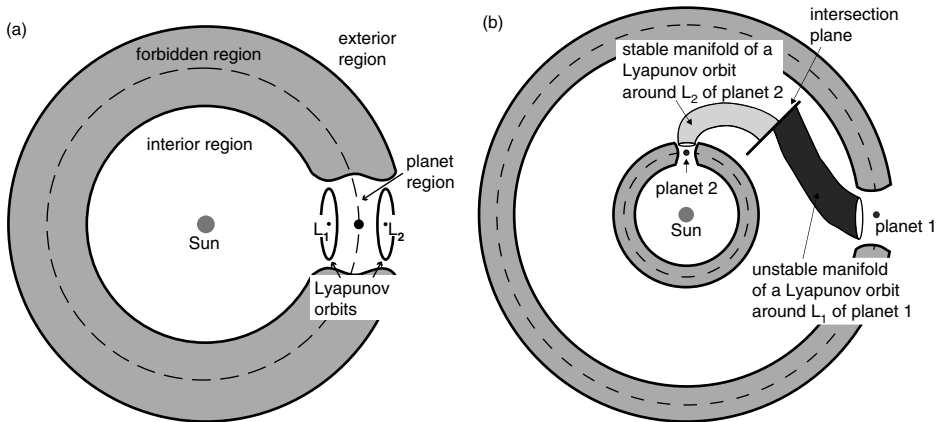

Fig. 5.1. Left: Projection of an energy surface onto position-space (schematic) for a value of the Jacobi integral for which the spacecraft is able to transit between the exterior and the interior region. Right: Sketch of the "patched 3-body approach" [26, 27]. The idea is to travel within certain invariant manifold "tubes", with possibly an impulsive correction maneuver at the intersection plane.

manifolds are cylinders that partition the three dimensional energy surface into two sets: (1) transit orbits, that locally pass between the *interior region* and the *planet region* in the case of an L_1-Lyapunov orbit or between the *exterior region* and the *planet region* in the case of L_2, and (2) non-transit orbits that stay in the exterior or interior region [30].

2. By "embedding" one PCR3BP into a second one, parts of the stable manifold of a Lyapunov orbit in one system may come close to the unstable manifold of a Lyapunov orbit in the other system (where, for a moment, it may help to imagine that the two systems do not move relative to each other), (Figure 5.1(b)). It may thus be possible for a spacecraft to "bridge the gap" between two pieces of trajectories in the vicinity of these manifolds by exerting an impulsive maneuver [26, 27].

One way to detect a close approach of two such invariant manifolds is to reduce the dimensionality of the problem. One computes the intersection of the two manifolds with a suitable intersection plane (Figure 5.1(b)) and determines points of close approach in this surface—for example by inspecting projections onto 2D-coordinate planes. This approach has in fact been used for a systematic construction of trajectories that follow prescribed itineraries around and between the Jovian moons [27]. In Section 5.6 of this chapter we go one step further and consider controlled problems via the incorporation of low thrust propulsion.

5.3 Set oriented numerics

Over the last decade *set oriented* numerical methods have been developed for the analysis of the global behavior of dynamical systems [6–10]. These numerical tools can, e.g., be used to approximate different types of invariant sets or invariant manifolds. They also allow to extract statistical information via the computation of natural invariant measures or almost invariant sets. In contrast to other numerical techniques these methods do not rely on the computation of *single long term* simulations but rather agglomerate the information obtained from *several short term* trajectories.

The methods are based on a multilevel subdivision procedure for the computation of certain invariant sets. This multilevel approach allows one to cover the object of interest—e.g., an invariant manifold or the support of an invariant measure—by several small subsets of state space. Since outer approximations are produced and long term simulations are avoided these methods are typically quite robust.

The numerical methods presented here are similar in spirit to the so-called *cell mapping approach* [22, 28]. However, there is a significant difference: the cell mapping approach relies on a partition of the *entire phase space* and thus the numerical effort depends crucially on its dimension. In contrast, in our set oriented apporach only a covering of the set of interest (e.g., the attractor) is constructed and so the computational effort essentially depends on the complexity of the underlying dynamics.

We would also like to mention that by now there exist several relevant extensions and adaptations of the set oriented approach as described here: the methods have been, e.g., combined with branch and bound techniques and methods from evolutionary optimization in order to solve global (multi-objective) optimization problems [13, 14, 33–35]. They

also have been combined with shortest path algorithms from graph theory in order to compute the optimal value function of optimal control problems as well as globally stabilizing feedback laws [19, 25].

5.3.1 The multilevel subdivision algorithm

We now describe the multilevel subdivision algorithm for the computation of invariant sets which forms the basis for all methods described in this chapter. We consider a discrete time dynamical system

$$x_{j+1} = f(x_j), \quad j = 0, 1, 2, \dots, \tag{5.3}$$

where $f: \mathbb{R}^n \to \mathbb{R}^n$ is a diffeomorphism which may, e.g., be given by the time-T-map of some underlying vector field.

A subset $A \subset \mathbb{R}^n$ is called *invariant* if

$$f(A) = A.$$

Moreover, an invariant set A is an *attracting set* with *fundamental neighborhood U* if for every open set $V \supset A$ there is an $N \in \mathbb{N}$ such that $f^j(U) \subset V$ for all $j \geq N$. Observe that if A is invariant then the closure of A is invariant as well. Hence we restrict our attention to closed invariant sets A, and in this case we obtain

$$A = \bigcap_{j \in \mathbb{N}} f^j(U).$$

By definition all the points in the fundamental neighborhood U are attracted by A. For this reason the open set $\cup_{j \in \mathbb{N}} f^{-j}(U)$ is called the *basin of attraction* of A. If the basin of attraction of A is the entire $\mathbb{R}^n$ then A is called the *global attractor*. Note that the global attractor contains all invariant sets of the given dynamical system.

Definition 5.3.1. Let $Q \subset \mathbb{R}^n$ be a compact set. We define the *global attractor relative to Q* by

$$A_Q = \bigcap_{j \geq 0} f^j(Q). \tag{5.4}$$

The definition of A_Q implies that $A_Q \subset Q$ and that $f^{-1}(A_Q) \subset A_Q$, but not necessarily that $f(A_Q) \subset A_Q$. Furthermore, A_Q is compact since Q is compact. Finally, A_Q is a subset of the global attractor A, however, in general $A_Q \neq A \cap Q$.

5.3.1.1 Subdivision algorithm

The following algorithm provides a method for the approximation of relative global attractors. It generates a sequence $\mathcal{B}_0, \mathcal{B}_1, \dots$ of finite collections of compact subsets of $\mathbb{R}^n$ such that the diameter $\text{diam}(\mathcal{B}_k) = \max_{B \in \mathcal{B}_k} \text{diam}(B)$ converges to zero for $k \to \infty$.

Given an initial collection $\mathcal{B}_0$, we inductively obtain $\mathcal{B}_k$ from $\mathcal{B}_{k-1}$ for $k = 1, 2, \ldots$ in two steps:

1. *Subdivision*: Construct a new collection $\hat{\mathcal{B}}_k$ such that

$$\bigcup_{B \in \hat{\mathcal{B}}_k} B = \bigcup_{B \in \mathcal{B}_{k-1}} B \tag{5.5}$$

   and

$$\mathrm{diam}(\hat{\mathcal{B}}_k) \leq \theta_k \, \mathrm{diam}(\mathcal{B}_{k-1}), \tag{5.6}$$

   where $0 < \theta_{\min} \leq \theta_k \leq \theta_{\max} < 1$.

2. *Selection*: Define the new collection $\mathcal{B}_k$ by

$$\mathcal{B}_k = \left\{ B \in \hat{\mathcal{B}}_k : \exists \hat{B} \in \hat{\mathcal{B}}_k \text{ such that } f^{-1}(B) \cap \hat{B} \neq \emptyset \right\}. \tag{5.7}$$

Note that by construction $\mathrm{diam}(\mathcal{B}_k) \leq \theta_{\max}^k \, \mathrm{diam}(\mathcal{B}_0) \to 0$ for $k \to \infty$.

Example 5.3.1.   We consider $f : \mathbb{R} \to \mathbb{R}$,

$$f(x) = \alpha x,$$

where $\alpha \in (0, \frac{1}{2})$ is a constant. Then the global attractor $A = \{0\}$ of f is a stable fixed point. We begin the subdivision procedure with $\mathcal{B}_0 = \{[-1, 1]\}$ and construct $\hat{\mathcal{B}}_k$ by bisection. In the first subdivision step we obtain

$$\mathcal{B}_1 = \hat{\mathcal{B}}_1 = \{[-1, 0], [0, 1]\}.$$

No interval is removed in the selection step, since each of them is mapped into itself. Now subdivision leads to

$$\hat{\mathcal{B}}_2 = \left\{ \left[-1, -\frac{1}{2}\right], \left[-\frac{1}{2}, 0\right], \left[0, \frac{1}{2}\right], \left[\frac{1}{2}, 1\right] \right\}.$$

Applying the selection rule (5.7), the two boundary intervals are removed, i.e.

$$\mathcal{B}_2 = \left\{ \left[-\frac{1}{2}, 0\right], \left[0, \frac{1}{2}\right] \right\}.$$

Proceeding this way, we obtain after k subdivision steps

$$\mathcal{B}_k = \left\{ \left[-\frac{1}{2^{k-1}}, 0\right], \left[0, \frac{1}{2^{k-1}}\right] \right\}.$$

We see that the union $\bigcup_{B \in \mathcal{B}_k} B$ is indeed approaching the global attractor $A = \{0\}$ for $k \to \infty$. The speed of convergence obviously depends on the contraction rate of the global attractor.

5.3.1.2 Convergence

The sequence of collections generated by the subdivision algorithm converges to the global attractor A_Q relative to Q. In addition to the following result one can also derive a statement about the speed of convergence in the case that the relative global attractor possesses a hyperbolic structure [8].

Proposition 5.3.1. *Let A_Q be the global attractor relative to the compact set Q, let $\mathcal{B}_0$ be a finite collection of closed subsets with $Q = \bigcup_{B \in \mathcal{B}_0} B$ and let $Q_k = \bigcup_{B \in \mathcal{B}_k} B$, $k = 0, 1, 2, \ldots$. Then*

$$\lim_{k \to \infty} h\left(A_Q, Q_k\right) = 0,$$

where $h(B, C)$ denotes the usual Hausdorff distance between two compact subsets $B, C \subset \mathbb{R}^n$ [8].

5.3.1.3 Implementation

We realize the closed subsets constituting the collections using generalized rectangles ("boxes") of the form

$$B(c, r) = \{y \in \mathbb{R}^n : |y_i - c_i| \le r_i \text{ for } i = 1, \ldots, n\},$$

where $c, r \in \mathbb{R}^n$, $r_i > 0$ for $i = 1, \ldots, n$, are the center and the radius, respectively. In the k-th subdivision step we subdivide each rectangle $B(c, r)$ of the current collection by bisection with respect to the j-th coordinate, where j is varied cyclically, i.e., $j = ((k-1) \bmod n) + 1$. This division leads to two rectangles $B_-(c^-, \hat{r})$ and $B_+(c^+, \hat{r})$, where

$$\hat{r}_i = \begin{cases} r_i & \text{for } i \neq j \\ r_i/2 & \text{for } i = j \end{cases}, \quad c_i^\pm = \begin{cases} c_i & \text{for } i \neq j \\ c_i \pm r_i/2 & \text{for } i = j \end{cases}.$$

Starting with a single initial rectangle we perform the subdivision until a prescribed size σ of the diameter relative to the initial rectangle is reached.

The collections constructed in this way can easily be stored in a binary tree. In Figure 5.2 we show the representation of three subdivision steps in three dimensions ($n = 3$) together with the corresponding sets Q_k, $k = 0, 1, 2, 3$. Note that each collection and the corresponding covering Q_k are completely determined by the tree structure and the initial rectangle $B(c, r)$.

5.3.1.4 Realization of the intersection test

In the subdivision algorithm we have to decide whether for a given collection $\mathcal{B}_k$ the image of a set $B \in \mathcal{B}_k$ has a non-zero intersection with another set $B' \in \mathcal{B}_k$, i.e., whether $f(B) \cap B' = \emptyset$. In simple model problems such as our trivial Example 5.3.1 this decision can be made analytically. For more complex problems we have to use some kind of discretization. Motivated by similar approaches in the context of cell-mapping techniques [22], we choose a finite set T of test points (on a grid or distributed randomly) in each set $B \in \mathcal{B}_k$ and replace the condition $f(B) \cap B' = \emptyset$ by $f(T) \cap B' = \emptyset$.

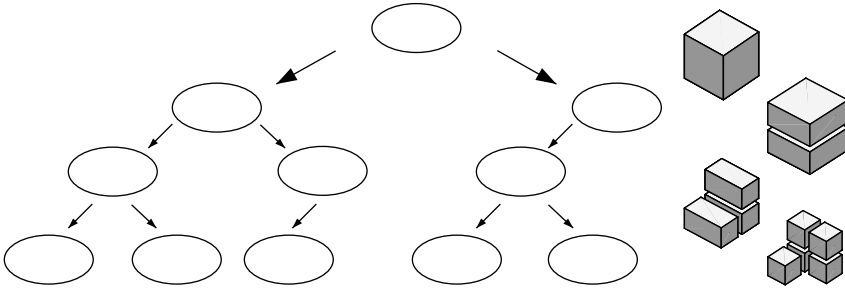Fig. 5.2. Storage scheme for the collections and the corresponding coverings Q_k, $k = 0, 1, 2, 3$.

Example 5.3.2.   Consider the Hénon map

$$f(x) = \begin{pmatrix} 1 - ax_1^2 + bx_2 \\ x_1 \end{pmatrix}. \tag{5.8}$$

for $b = 0.2$ and $a = 1.2$. Starting with the square $Q = [-2, 2]^2$, we display in Figure 5.3 the coverings of the global attractor relative to Q obtained by the algorithm after 8 and 12 subdivision steps.

The figures have been generated by the following GAIO script:

```
addpath(strcat(getenv('GAIODIR'),'/matlab'))
henon = Model('ohenon');
map = Integrator('Map');
map.model = henon;
henon.a = 1.2;
henon.b = 0.2;
```
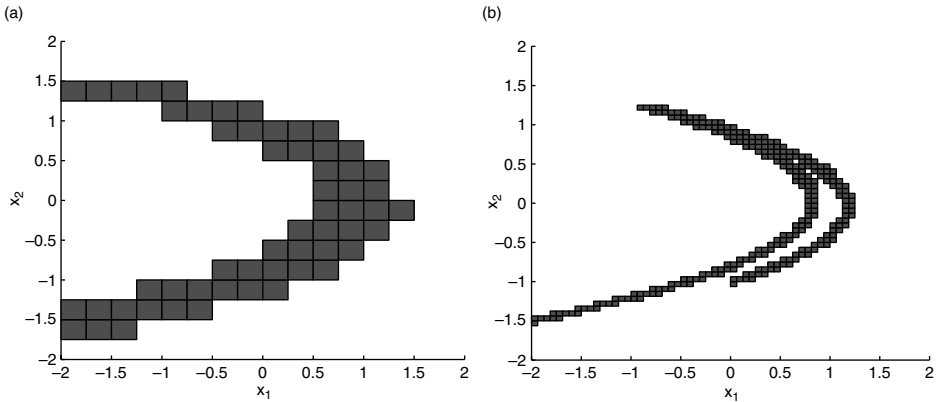

Fig. 5.3. Coverings of the global Hénon attractor after 8 (left) and 12 (right) subdivision steps.
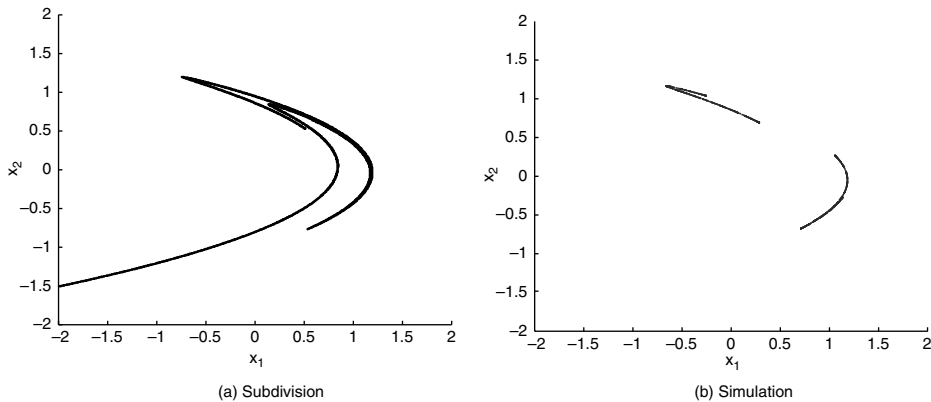
(a) Subdivision

(b) Simulation

Fig. 5.4. (a) Approximation of the relative global attractor for the Hénon mapping after 18 subdivision steps; (b) attractor of the Hénon mapping computed by direct simulation.

```
edges = Points('Edges', 2, 100);
center = Points('Center', 2, 1);
tree = Tree([0 0], [2 2]);
tree.integrator = map;
tree.domain_points = edges;
tree.image_points = center;
rga(tree,8);
plotb(tree);
rga(tree,4);
clf; plotb(tree);
```

In Figure 5.4(a) we show the rectangles covering the relative global attractor after 18 subdivision steps. Note that a direct simulation would not yield a similar result. In Figure 5.4(b) we illustrate this fact by showing a trajectory, neglecting the transient behavior. This difference is due to the fact that the subdivision algorithm covers all invariant sets in Q, together with their unstable manifolds. In particular, the one-dimensional unstable manifolds of the two fixed points are approximated—but those cannot be computed by direct simulation.

5.4 Computing invariant manifolds

We now present a set oriented method for the computation of invariant manifolds. Although the method can in principle be applied to manifolds of arbitrary hyperbolic invariant sets we will restrict, for simplicity, to the case of a hyperbolic fixed point p.

We fix a (large) compact set $Q \subset \mathbb{R}^n$ containing p, in which we want to approximate part of the global unstable manifold $W^u(p)$ of p. To combine the subdivision algorithm

with a continuation method, we realize the subdivision process using a nested sequence $\mathcal{P}_\ell$, $\ell \in \mathbb{N}$, of successively finer finite partitions of Q, i.e., for all $B \in \mathcal{P}_{\ell+1}$ there exist $B' \in \mathcal{P}_\ell$ such that $B \subset B'$ and $\operatorname{diam}(B) \leq \theta \operatorname{diam}(B')$ for some $0 < \theta < 1$.

Let $C \in \mathcal{P}_\ell$ be a neighborhood of the hyperbolic fixed point p such that the global attractor relative to C satisfies

$$A_C = W^u_{\text{loc}}(p) \cap C.$$

Applying k steps of the subdivision algorithm to $\mathcal{B}_0 = \{C\}$, we obtain a covering $\mathcal{B}_k \subset \mathcal{P}_{\ell+k}$ of the local unstable manifold $W^u_{\text{loc}}(p) \cap C$. By Proposition 3.1, this covering converges to $W^u_{\text{loc}}(p) \cap C$ for $k \to \infty$. The following algorithm grows this initial covering until it covers a certain subset of the global unstable manifold of p.

5.4.1 Continuation algorithm

For a fixed k we define a sequence $\mathcal{C}_0^{(k)}, \mathcal{C}_1^{(k)}, \ldots$ of subsets $\mathcal{C}_j^{(k)} \subset \mathcal{P}_{\ell+k}$ by

1. *Initialization*:

$$\mathcal{C}_0^{(k)} = \mathcal{B}_k.$$

2. *Continuation*: For $j = 0, 1, 2, \ldots$ define

$$\mathcal{C}_{j+1}^{(k)} = \left\{ B \in \mathcal{P}_{\ell+k} : B \cap f(B') \neq \emptyset \text{ for some } B' \in \mathcal{C}_j^{(k)} \right\}.$$

Observe that the sets $C_j^{(k)} = \bigcup_{B \in \mathcal{C}_j^{(k)}} B$ form nested sequences in k, i.e., $C_j^{(0)} \supset C_j^{(1)} \supset \ldots$ for $j = 0, 1, 2, \ldots$.

5.4.2 Convergence result and error estimate

Set $W_0 = W^u_{\text{loc}}(p) \cap C$ and define inductively for $j = 0, 1, 2, \ldots$

$$W_{j+1} = f(W_j) \cap Q.$$

Proposition 5.4.1. *[7]. The sets $C_j^{(k)}$ are coverings of W_j for all $j, k = 0, 1, \ldots$. Moreover, for fixed j, $C_j^{(k)}$ converges to W_j in Hausdorff distance if the number k of subdivision steps in the initialization goes to infinity.*

It can in general not be guaranteed that the continuation method leads to an approximation of the entire set $W^u(p) \cap Q$. The reason is that the unstable manifold of the hyperbolic fixed point p may "leave" Q but may as well "wind back" into it.

If we additionally assume the existence of a hyperbolic structure along the unstable manifold then we can establish results on the convergence behavior of the continuation method in a completely analogous way as in Ref. [8]. To this end assume that p is an element of an attractive hyperbolic set A. Then the unstable manifold of p is contained in A. We choose $Q = \overline{\bigcup_{x \in A} W^s_\eta(x)}$ for some sufficiently small $\eta > 0$, such that $A = A_Q$.

Let $\rho \geq 1$ be a constant such that for every compact neighborhood $\widetilde{Q} \subset Q$ of A_Q we have $h(A_Q, \widetilde{Q}) \leq \delta \Rightarrow \widetilde{Q} \subset U_{\rho\delta}(A_Q)$.

Proposition 5.4.2. *[23]. Assume that in the initialization step of the continuation method we have*

$$h(W_0, C_0^{(k)}) \leq \zeta \operatorname{diam} C_0^{(k)}$$

for some constant $\zeta > 0$. If $C_j^{(k)} \subset W_\eta^s(W_j)$ for $j = 0, 1, 2, \ldots, J$, then

$$h(W_j, C_j^{(k)}) \leq \operatorname{diam} C_j^{(k)} \max\left(\zeta, 1 + \beta + \beta^2 + \cdots + \beta^j \zeta\right) \tag{5.9}$$

for $j = 1, 2, \ldots, J$. Here $\beta = C\lambda\rho$ and C and λ are the characteristic constants of the hyperbolic set A.

The estimate (5.9) points up the fact that for a given initial level k and λ near 1—corresponding to a weak contraction transversal to the unstable manifold—the approximation error may increase dramatically with an increasing number of continuations steps (i.e., increasing j).

Example 5.4.1. As a numerical example we consider the (spatial) circular restricted three-body problem (Section 5.2) with $\mu = 3.040423398444176 \times 10^{-6}$ for the Sun/Earth system.

Motivated by the requirements of the mission design for the *NASA Genesis discovery mission* we aim for the computation of the unstable manifold of a certain unstable periodic orbit (a so-called *halo orbit*) in the vicinity of the L_1 Lagrange point. In light of Proposition 5.4.2, a naive application of the continuation method would—due to the Hamiltonian nature of the system—not lead to satisfactory results in this case. We therefore apply a modified version of this method [23]. Roughly speaking the idea is not to continue the current covering by considering *one* application of the map at *each* continuation step, but instead to perform only *one* continuation step while computing *several* iterates of the map.

More formally, we replace the second step in the continuation method by:

(ii) *Continuation*: For some $J > 0$ define

$$C_J^{(k)} = \left\{ B \in \mathcal{P}_{\ell+k} : \exists \, 0 \leq j \leq J : B \cap f^j(B') \neq \emptyset \text{ for some } B' \in C_0^{(k)} \right\}.$$

The convergence statement in Proposition 5.4.1 is adapted to this method in a straightforward manner. One can also show that—as intended—the Hausdorff-distance between compact parts of the unstable manifold and the computed covering is of the order of the diameter of the partition, see Ref. [23] for details. However, and this is the price one has to pay, one no longer considers short term trajectories here and therefore accumulates methodological and round-off errors when computing the iterates f^j.

A second advantage of the modified continuation method is that whenever the given dynamical system stems from a flow ϕ^t one can get rid of the necessity to consider a time-T-map and instead replace the continuation step by

(ii) *Continuation*: For some $T > 0$ define

$$\mathcal{C}_T^{(k)} = \left\{ B \in \mathcal{P}_{\ell+k} : \exists\, 0 \le t \le T : B \cap \phi^t(B') \neq \emptyset \text{ for some } B' \in \mathcal{C}_0^{(k)} \right\}.$$

This facilitates the usage of integrators with adaptive step-size control and finally made the computations feasible for this example. Figure 5.5 shows the result of the computation, where we set $T = 7$ and used an embedded Runge-Kutta scheme of order 8 as implemented in the code DOPRI853[2] [21] with error tolerances set to 10^{-9}. See again [23] for more details on this computation. A movie illustrating a flight along this manifold is available at http://www-math.upb.de/~agdellnitz/Software/halo.html.
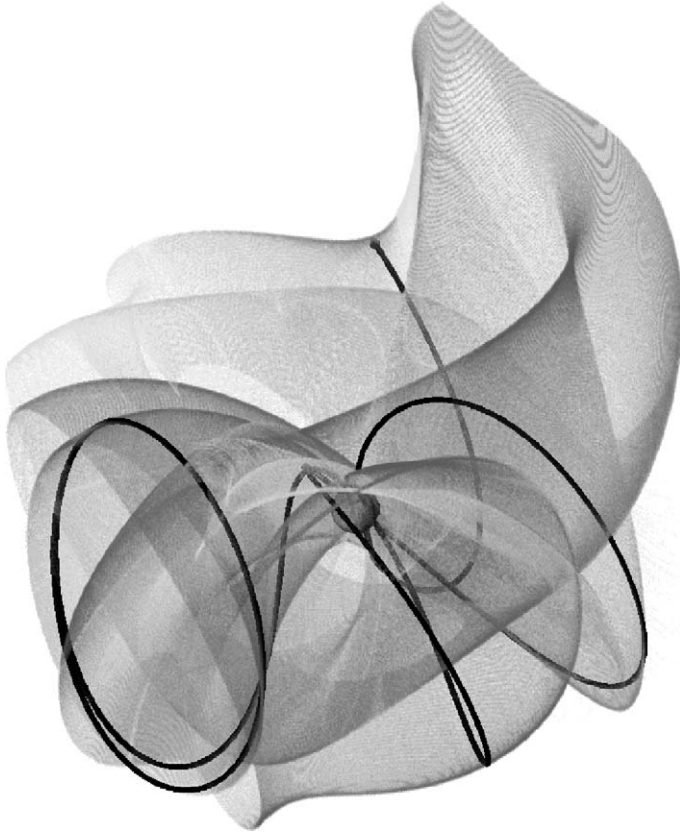

Fig. 5.5. Covering of part of the global unstable manifold of an unstable periodic orbit in the circular restricted three-body problem (projection onto configuration space). The blue body depicts the Earth, the black trajectory is a sample orbit which leaves the periodic orbit in the direction of the Earth. The coloring indicates the temporal distance from the periodic orbit. (see Color plate 1)

---

[2] `http://www.unige.ch/~hairer/software.html`.

5.5 Detecting connecting orbits

One of the key ideas in applying dynamical systems techniques in space mission design is to use *connecting orbits* between different invariant sets (e.g., periodic orbits or invariant tori) as energy efficient trajectories for the spacecraft.

In this section we show how the set oriented continuation algorithm for the computation of invariant manifolds described in the previous section can be used in order to detect connecting orbits. For simplicity, we restrict our considerations to the situation where connecting orbits between different steady state solutions have to be detected. We consider a parameter dependent ordinary differential equation

$$\dot{x} = f(x, \lambda), \tag{5.10}$$

where $f: \mathbb{R}^d \times \Lambda \to \mathbb{R}^d$ is a smooth vector field and $\Lambda \subset \mathbb{R}$ is an interval. Denote by x_λ and y_λ, $\lambda \in \Lambda$, two one-parameter families of hyperbolic steady state solutions of (5.10)—allowing that $x_\lambda = y_\lambda$. We are interested in the detection of a connecting orbit between two steady states $x_{\bar{\lambda}}$, $y_{\bar{\lambda}}$ while the system parameter λ is varied. In order to ensure that, in principle, connecting orbits can generically occur we assume that

$$\dim(W^u(x_\lambda)) + \dim(W^s(y_\lambda)) = d \quad \text{for all } \lambda \in \Lambda.$$

Here $W^u(x_\lambda)$ and $W^s(y_\lambda)$ denote the unstable resp. the stable manifold of the corresponding steady states.

We do not just aim for a rough guess of the parameter value $\bar{\lambda}$ but also for a guess of the connecting orbit itself. Using these data as initial values one may employ standard techniques on the computation of hetero-/homoclinic orbits [3, 17].

The discrete dynamical system which we are considering is the time-τ map of the flow of (5.10). We approximate this map using an explicit numerical integration scheme and denote by $\mathcal{U}_j^{(k)}(\lambda)$ and $\mathcal{S}_j^{(k)}(\lambda)$ the covering of the unstable resp. the stable manifold of x_λ resp. y_λ obtained by the continuation algorithm (Section 5.4) after k subdivision and j continuation steps. Let

$$\mathcal{I}_j^{(k)}(\lambda) = \mathcal{U}_j^{(k)}(\lambda) \cap \mathcal{S}_j^{(k)}(\lambda).$$

The idea of the following algorithm is to find intersections of the box coverings $\mathcal{U}_j^{(k)}(\lambda)$ and $\mathcal{S}_j^{(k)}(\lambda)$ for different values of λ and k. Using the hierarchical data structure introduced in Section 5.3 these intersections can efficiently be computed. In fact, both coverings are stored within the same tree and boxes belonging to different coverings are marked by different flags. The boxes which belong to both coverings are then easily identified as those that are marked by both flags.

Roughly speaking we are going to use the fact that if there exists a connecting orbit for $\lambda = \bar{\lambda}$, then the smaller the distance $|\lambda - \bar{\lambda}|$ the bigger we can choose the number of subdivisions k while still finding a non-empty intersection $\mathcal{I}_j^{(k)}(\lambda)$. That is, if we plot the maximal k for which a non-empty intersection is found versus λ, we expect to see a schematic picture as illustrated in Figure 5.6.
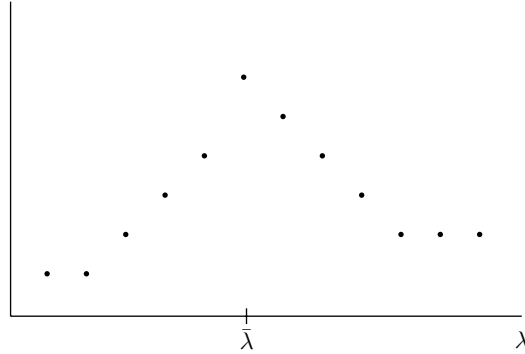
Fig. 5.6. Maximal number of subdivisions k for which an intersection of the coverings $\mathcal{U}_j^{(k)}(\lambda)$ and $\mathcal{S}_j^{(k)}(\lambda)$ has been found versus the parameter λ (schematic).

5.5.1 The hat algorithm

Let $\tilde{\Lambda} \subset \Lambda$ be a finite set of parameter values—e.g., a set of equidistant values of λ inside Λ. Taking $\tilde{\Lambda}$, $k_{\max} \in \mathbb{N}$ and $j_{\max} \in \mathbb{N}$ as inputs the following algorithm computes a function $m : \tilde{\Lambda} \to \mathbb{N}$ such that local maximizers of m are close to parameter values $\bar{\lambda}$ for which there may exist a connecting orbit between $x_{\bar{\lambda}}$ and $y_{\bar{\lambda}}$.

```
m = hat(Λ̃, k_max, j_max)
for all λ ∈ Λ̃
    k:=0
    do
        j:=0
        do
            compute 𝒰ⱼ⁽ᵏ⁾(λ) and 𝒮ⱼ⁽ᵏ⁾(λ)
            j:=j+1
        while 𝒥ⱼ⁽ᵏ⁾(λ) = ∅ and k<j_max
        k:=k+1
    while 𝒥ⱼ⁽ᵏ⁾(λ) ≠ ∅ and k<j_max
    m(λ) =k
end
```

In the case where $x_\lambda = y_\lambda$ one obviously has a non-empty intersection of $\mathcal{U}_j^{(k)}(\lambda)$ and $\mathcal{S}_j^{(k)}(\lambda)$ for all $\lambda \in \Lambda$. In this case one needs to modify the intersection test accordingly. In practice this is done by excluding parts of the box coverings which are inside some neighborhood of the steady state solution x_λ.

We now show that the hat algorithm can indeed be used for the detection of non-degenerate heteroclinic co-dimension one bifurcations [20]. Let ϕ^t denote the flow of the system (5.10). Then we define for an equilibrium p and $T \geq 0$

$$W_T^u(p) = \bigcup_{0 \leq t \leq T} \phi^t(W_{\mathrm{loc}}^u(p)), \qquad W_T^s(p) = \bigcup_{-T \leq t \leq 0} \phi^t(W_{\mathrm{loc}}^s(p)),$$

where $W_{\text{loc}}^{u,s}(p)$ are local (un)stable manifolds of p. If there exists an orbit connecting x_λ and y_λ for $\lambda = \bar{\lambda}$ then there is a $T \geq 0$ such that

$$W_T^u(x_{\bar{\lambda}}) \cap W_T^s(y_{\bar{\lambda}}) \neq \emptyset.$$

(In practice, the minimal T with this property is unknown and this is the reason why one should choose a rather large value for the parameter j_{max} in the input of the hat algorithm.) Accordingly the intersection $\mathcal{I}_j^{(k)}(\bar{\lambda})$ will be non-empty for all box coverings $\mathcal{U}_j^{(k)}(\bar{\lambda})$ and $\mathcal{S}_j^{(k)}(\bar{\lambda})$ satisfying

$$W_T^u(x_{\bar{\lambda}}) \subset \bigcup_{B \in \mathcal{U}_j^{(k)}(\bar{\lambda})} B \quad \text{and} \quad W_T^s(x_{\bar{\lambda}}) \subset \bigcup_{B \in \mathcal{S}_j^{(k)}(\bar{\lambda})} B.$$

In fact since there exists a connecting orbit for $\lambda = \bar{\lambda}$, $\mathcal{I}_j^{(k)}(\bar{\lambda})$ will be non-empty for all k if j is big enough. But also the converse is true:

Proposition 5.5.1. *[12]. If for some $\bar{\lambda} \in \tilde{\Lambda}$ and $j \in \mathbb{N}$ the intersection $\mathcal{I}_j^{(k)}(\bar{\lambda})$ is non-empty for all k, then there exists an orbit of (5.10) connecting $x_{\bar{\lambda}}$ and $y_{\bar{\lambda}}$.*

For the statement of the following result it is convenient to introduce a specific choice for the set $\tilde{\Lambda}$. If $\Lambda = [a, b]$ then we define for $n \in \mathbb{N}$

$$h = \frac{b-a}{n} \quad \text{and} \quad \tilde{\Lambda}_h = \{a + ih : i = 0, 1, \ldots, n\}.$$

Proposition 5.5.2. *Suppose that for some $\bar{\lambda} \in \Lambda$ the system (5.10) undergoes a non-degenerate heteroclinic co-dimension one bifurcation with respect to the steady state solutions x_λ and y_λ. Then for each integer $k_{max} > 0$ there are $h > 0$ and $j_{max} > 0$ such that those $\tilde{\lambda} \in \tilde{\Lambda}_h$ for which $|\tilde{\lambda} - \bar{\lambda}|$ is minimal satisfy $m(\tilde{\lambda}) = k_{max}$. These values are in particular local maximizers of $m : \tilde{\Lambda} \to \mathbb{N}$. (Here m denotes the function computed by the hat algorithm.)*

Proof. Suppose that j_{max} is chosen in such a way that $\mathcal{I}_j^{(k)}(\bar{\lambda})$ is non-empty for all k and $j = j_{max} - 1$. Then, by construction of the hat algorithm, $m(\bar{\lambda}) = k_{max}$. Since $W_T^u(x_\lambda)$ and $W_T^s(y_\lambda)$ depend continuously on λ we can conclude that there is an $\eta > 0$ such that $m(\lambda) = k_{max}$ for all $\lambda \in (\bar{\lambda} - \eta, \bar{\lambda} + \eta)$. Now choose $h > 0$ so small that $\tilde{\Lambda}_h \cap (\bar{\lambda} - \eta, \bar{\lambda} + \eta) \neq \emptyset$. $\qquad\square$

5.5.2 Numerical examples

Consider the system [4]

$$\begin{aligned} \dot{x} &= y \\ \dot{y} &= -\lambda y + x^3 + x^2 - 3x + 1. \end{aligned} \tag{5.11}$$

Our aim is to detect an orbit within the region $[-3, 2] \times [-3, 3]$ which connects the equilibrium $x_\lambda = (-1 - \sqrt{2}, 0)$ to the equilibrium $y_\lambda = (1, 0)$. We use the time-0.2-map of
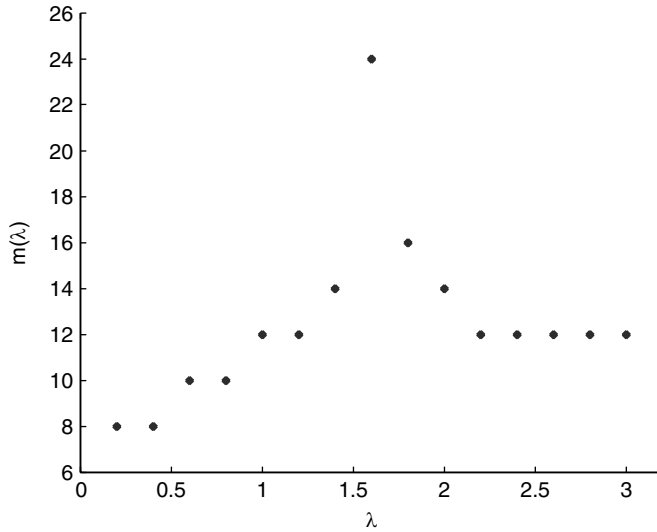
Fig. 5.7. The function m for system (5.11).

the corresponding flow and choose $\tilde{\Lambda} = \{0.2, 0.4, 0.6, \dots, 2.8, 3.0\}$, as well as $k_{max} = 26$ and $j_{max} = 20$ as inputs for the hat algorithm. Figure 5.7 shows the graph of the resulting function m. It indicates that for $\lambda \approx 1.6$ there indeed exists a connecting orbit.

In order to illustrate the behavior of the hat algorithm we additionally show the box coverings obtained (a) for a fixed parameter value $\lambda = 1.6$ and for different numbers of subdivisions k (Figure 5.8) and (b) for a fixed depth $k = 14$ and different parameter values λ (Figure 5.9).
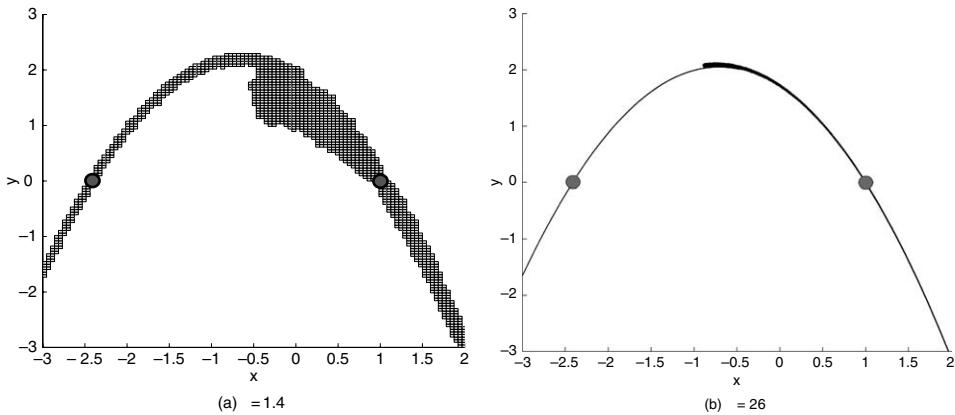

(a) $k = 1.4$

(b) $k = 26$

Fig. 5.8. The coverings $\mathcal{U}^{(k)}(1.6)$ and $\mathcal{S}^{(k)}(1.6)$ for different k. The two equilibria are marked by dots.
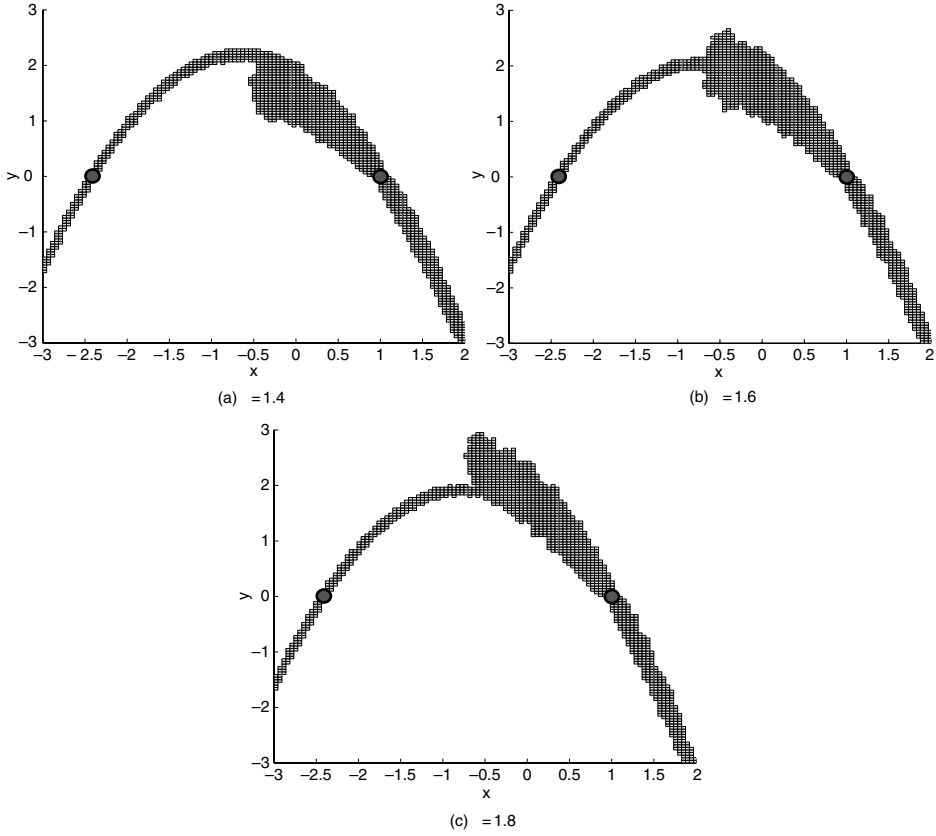
(a) = 1.4

(b) = 1.6

(c) = 1.8

Fig. 5.9. The coverings $\mathcal{U}^{(14)}(\lambda)$ and $\mathcal{S}^{(14)}(\lambda)$ in dependence on λ.

5.5.3 The Lorenz system

As a second example we consider the Lorenz system

$$\dot{x} = \sigma(y - x)$$
$$\dot{y} = \rho x - y - xz$$
$$\dot{z} = xy - \beta z$$

with parameter values $\sigma = 10$ and $\beta = \frac{8}{3}$. It is well known that there exists a homoclinic orbit for the origin near $\rho = 13.93$ [36]. We consider the time-T map of the corresponding flow with $T = 0.2$ and apply the hat algorithm with $\tilde{\Lambda} = \{7, 8, 9, \ldots, 19, 20\}$, $k_{max} = 30$ and $j_{max} = 8$. Figure 5.10 shows the result of this computation as well as the number of boxes in the intersection of $\mathcal{U}^{(27)}(\rho)$ and $\mathcal{S}^{(27)}(\rho)$ for $\rho \in \{13, 13.5, 14, 14.5, 15\}$. Again we illustrate the computations by plotting several computed coverings, see Figures 5.11 and 5.12.
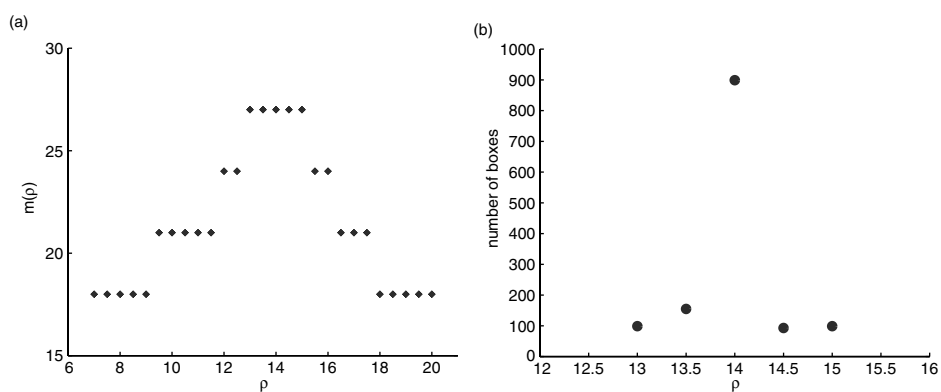
Fig. 5.10. Results for the Lorenz system. Left: The function m. Right: The number of boxes in $\mathcal{J}^{(27)}(\rho)$ as a function of ρ.
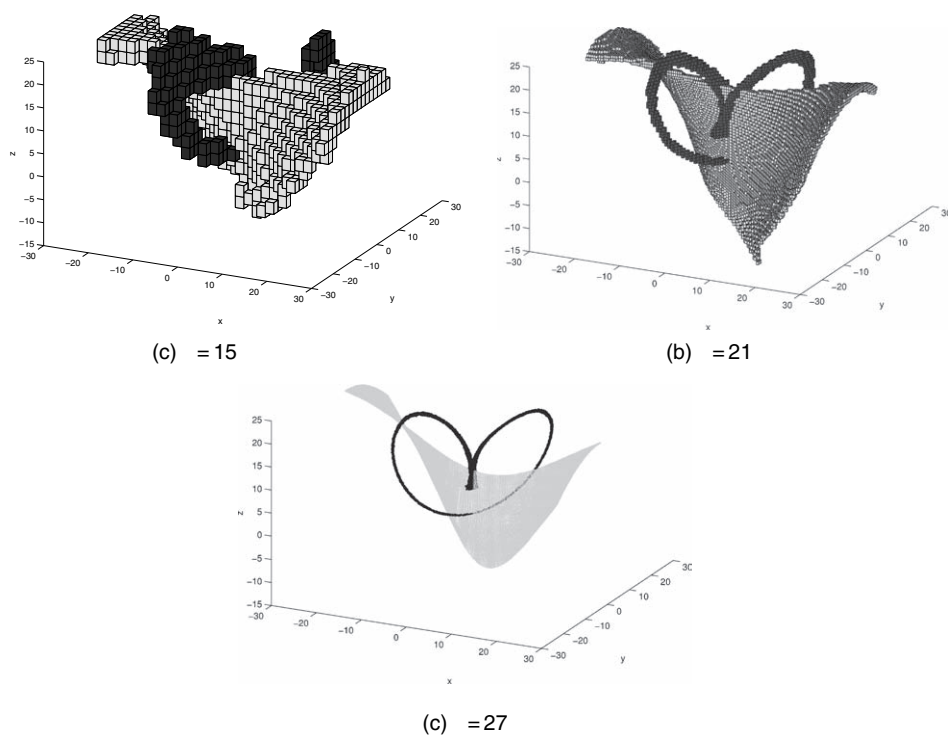

Fig. 5.11. Lorenz system: The coverings $\mathcal{U}_{(k)}(14)$ (blue) and $\mathcal{S}_{(k)}(14)$ (yellow) for different k. (see Color plate 2)
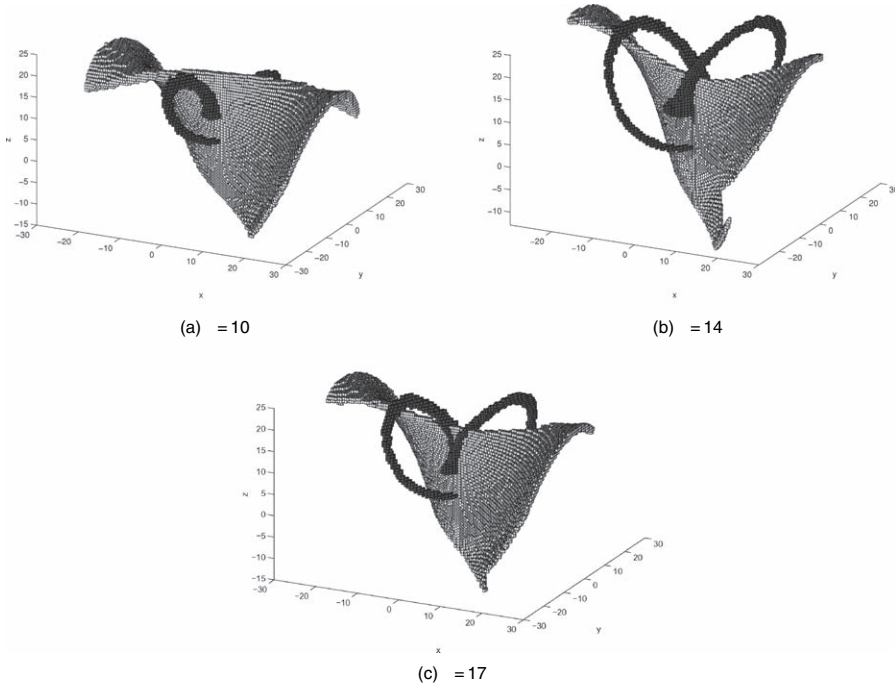
(a) = 10

(b) = 14

(c) = 17

Fig. 5.12. Lorenz system: The coverings $\mathcal{U}^{(21)}(\rho)$ (blue) and $\mathcal{S}^{(21)}(\rho)$ (yellow) in dependence of ρ. (see Color plate 3)

5.6 Extension to controlled systems

The "patched 3-body approach" for the construction of energy efficient trajectories as sketched in Section 5.2 is tailored for spacecraft with impulsive thrusters. In this section, we propose an extension of this approach to the case of continuously controlled spacecraft (as realized by certain low thrust propulsion systems). Roughly speaking, the stable and unstable manifold tubes are replaced by certain (forward and backward) reachable sets in phase space. Using set oriented numerical tools it is possible to efficiently compute coverings of these sets as well as of the intersection of them with suitably chosen cross sections. We illustrate the approach by considering a low thrust mission to Venus.

5.6.1 A controlled three-body problem

In current mission concepts, like for the ESA interplanetary mission *BepiColombo* to Mercury or the *Smart I* mission, ion propulsion systems are being used that continuously exert a small force on the spacecraft ("low-thrust propulsion"). In order to model the motion of these spacecraft, we amend the planar circular restricted three-body problem (5.1) by a suitably defined control term. We restrict our considerations to the special case

of a control force whose direction is defined by the spacecraft's velocity such that the control term is parametrized by a single real value u, determining the magnitude of the control acceleration. We do not take into account here that the mass of the spacecraft changes during its flight.

The velocity vector of the spacecraft has to be viewed with respect to the inertial coordinate system and not the rotating one. In view of this, one is lead to the following control system (Figure 5.13):

$$\ddot{x} + 2\dot{x}^\perp = \nabla\Omega(x) + u\,\frac{\dot{x} + \omega x^\perp}{\|\dot{x} + \omega x^\perp\|}. \tag{5.12}$$

Here, $u = u(t) \in [u_{min}, u_{max}] \subset \mathbb{R}$ denotes the magnitude of the control force, $x = (x_1, x_2)$, $x^\perp = (-x_2, x_1)$ and ω is the common angular velocity of the primaries.

In a mission to Venus the spacecraft will get closer to the Sun, meaning that part of its potential energy with respect to the Sun will be transformed into kinetic energy. As a consequence, the spacecraft's velocity will have to be reduced during its flight such that it matches the one of Venus. Thus, in our concrete application the control values u will actually be negative.

5.6.2 Coupling controlled three-body problems

Obviously, every solution of (5.1) is also a solution of (5.12) for the control function $u \equiv 0$. We are going to exploit this fact in order to generalize the patched three-body approach as described in Section 5.2.2 to the case of controlled three-body problems. We are still going to use the L_1- and L_2-Lyapunov orbits as "gateways" for the transition between the interior, the planet, and the exterior regions. However, instead of computing the relevant invariant manifolds of these periodic orbits, we compute certain *reachable sets* [5], i.e., sets in phase space that can be accessed by the spacecraft when employing a certain control function.

5.6.2.1 Reachable sets

We denote by $\phi(t, z, u)$ the solution of the control system (5.12) for a given initial point $z = (x, \dot{x})$ in phase space and a given admissible control function $u \in \mathcal{U} = \{u : \mathbb{R} \to$
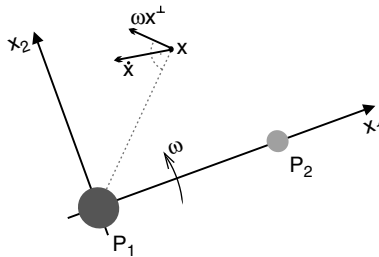

Fig. 5.13. The velocity of the spacecraft with respect to the inertial frame is given by $\dot{x} + \omega x^\perp$.

$[u_{\min}, u_{\max}]$, u admissible}. The set of admissible control functions will be determined by the design of the thrusters. For example, it could consist of piecewise constant functions, where the minimal length of an interval on which the function is constant is determined by how fast the magnitude of the accelerating force can be changed within the thrusters.

For a set S in phase space and a given function $\tau : S \times \mathcal{U} \to \mathbb{R}$, we call $\mathcal{R}(S, \tau) = \{\phi(\tau(x, u), x, u) \mid u \in \mathcal{U}, x \in S\}$ the set which is (τ-) *reachable from S*.

5.6.2.2 Patched controlled three-body systems

We now extend the patched three-body approach to the context of a controlled system.

Roughly speaking, the extension can be summarized as follows: For two suitable subsets $\mathcal{O}_1$ and $\mathcal{O}_2$ in phase space (typically two sets in the vicinity of an L_1–Lyapunov orbit of the outer planet and an L_2–Lyapunov orbit of the inner one, respectively) one computes associated reachable sets $\mathcal{R}_1 \subset \Sigma_1$ and $\mathcal{R}_2 \subset \Sigma_2$ within suitably chosen intersection planes Σ_1 and Σ_2 in each system. After a transformation of one of these reachable sets into the other rotating system, one determines their intersection. By construction, points in this intersection define trajectories that link the two "gateway sets" $\mathcal{O}_1$ and $\mathcal{O}_2$.

More precisely, the procedure is as follows:

1. Identify suitable sets $\mathcal{O}_1$ and $\mathcal{O}_2$ in the phase space of the two three-body problems, respectively. They should be chosen such that all points in $\mathcal{O}_1$ belong to trajectories that transit from the planet region into the interior region (of the outer planet) and those in $\mathcal{O}_2$ transit from the exterior region to the planet region (of the inner planet). Furthermore, in each of the two three-body problems, choose an intersection plane $\Sigma_i = \{\theta = \theta_i\}$, $i = 1, 2$, (where (r, θ) are polar coordinates for the position of the spacecraft and θ_i is a suitable angle, see also step 3). Typically the sets $\mathcal{O}_1$ and $\mathcal{O}_2$ will lie close to certain Lyapunov orbits.

2. For points $x_1 \in \mathcal{O}_1$ and $x_2 \in \mathcal{O}_2$ and an admissible control function u, let

$$\tau_1(x_1, u) = \inf\{t > 0 \mid \phi(t, x_1, u) \in \Sigma_1\} \quad \text{and}$$

$$\tau_2(x_2, u) = \sup\{t < 0 \mid \phi(t, x_2, u) \in \Sigma_2\}.$$

For $i = 1, 2$, compute

$$\mathcal{R}(\mathcal{O}_i, \tau_i) = \{\phi(\tau_i(x, u), x, u) \mid x \in \mathcal{O}_i, u \in \mathcal{U}\} \subset \Sigma_i. \tag{5.13}$$

3. In order to transform one of the reachable sets $\mathcal{R}(\mathcal{O}_1, \tau_1)$ or $\mathcal{R}(\mathcal{O}_2, \tau_2)$ into the other rotating frame, let $\theta(t)$ be the phase angle between the two planets as seen in the rotating frame of the inner planet. Choose a time t_0 such that $\theta(t_0) = \theta_1 - \theta_2$. (Alternatively, based on a prescribed time t_0, one could choose the section angles θ_1 and θ_2 in step 1 such that $\theta(t_0) = \theta_1 - \theta_2$.) Using t_0, transform $\mathcal{R}(\mathcal{O}_1, \tau_1)$ into the rotating frame of the inner planet, yielding the set $\hat{\mathcal{R}}(\mathcal{O}_1, \tau_1) \subset \Sigma_2$. Note that here we exploit the fact that both systems are autonomous.

4. Compute the intersection (see below)

$$\hat{\mathcal{R}}(\mathcal{O}_1, \tau_1) \cap \mathcal{R}(\mathcal{O}_2, \tau_2) \subset \Sigma_2. \tag{5.14}$$

By construction, for each point $x \in \hat{\mathcal{R}}(\mathcal{O}_1, \tau_1) \cap \mathcal{R}(\mathcal{O}_2, \tau_2)$, there exist admissible control functions u_1 and u_2 and times $t_1 = -\tau(\tilde{x}, u_1)$, $t_2 = -\tau(\bar{x}, u_2)$, such that $\phi(t_1, \tilde{x}, u_1) \in \mathcal{O}_1$

and $\phi(t_2, x, u_2) \in \mathcal{O}_2$, where $\tilde{x}$ are the coordinates of x with respect to the rotating frame of the outer planet at the phase angle $\theta(t_0)$ between the two planets. By construction of the sets $\mathcal{O}_1$ and $\mathcal{O}_2$ we have thus found a controlled trajectory that transits from the outer planet region into the inner planet region.

5.6.2.3 Implementation

Let $\mathcal{P}$ be a finite partition of some relevant bounded part of Σ_2. We compute coverings $\mathcal{P}_1, \mathcal{P}_2 \subset \mathcal{P}$ of $\hat{\mathcal{R}}(\mathcal{O}_1, \tau_1)$ and $\mathcal{R}(\mathcal{O}_2, \tau_2)$ by integrating a finite set of test points in $\mathcal{O}_1$ and $\mathcal{O}_2$, respectively. In the example computations, we restrict ourselves to constant control functions with values in a grid in $[u_{\min}, u_{\max}]$. For each of these values and each test point, we numerically integrate the control system (5.12) by an embedded Runge-Kutta scheme with adaptive stepsize control as implemented in the code DOP853 by Hairer and Wanner [21]. After each integration step, we check whether the computed trajectory has crossed the intersection plane Σ_1 resp. Σ_2 and, if this is the case, start Newton's method in order to obtain a point in the intersection plane. In the case of $\hat{\mathcal{R}}(\mathcal{O}_1, \tau_1)$, we transform this point into the other system and, in both cases, add the corresponding partition element to the collection $\mathcal{P}_1$ resp. $\mathcal{P}_2$.

Analogously to the approach in Section 5.5, we then extract all partition elements P from $\mathcal{P}$ which belong to both coverings. In each element, we furthermore store the minimal Δv that is necessary to reach this set from either $\mathcal{O}_1$ or $\mathcal{O}_2$. Whenever the intersection $\mathcal{P}_1 \cap \mathcal{P}_2$ consists of more than one partition element, this enables us to choose trajectories with a minimal Δv (with respect to the chosen parameters).

5.6.2.4 Application for a mission to venus

We now apply the approach described in the previous paragraphs to the design of a mission to Venus. In 2005, the European Space Agency has launched *VenusExpress*[3], a mission to Venus that sends a *MarsExpress*-like spacecraft into an elliptical orbit around Venus via a Hohmann transfer. Transfer time from Earth is around 150 days, while the required Δv amounts to roughly 1500 m/s [1, 18]. The interplanetary low-thrust orbit that we are going to construct now corresponds to a flight time of roughly 1.4 years, applying a Δv of approximately 3300 m/s. Since typical low-thrust propulsion systems (as in the ESA mission *Smart I* and the planned cornerstone mission *BepiColombo* for example) have a specific impulse which is approximately an order of magnitude larger than the one of chemical engines, these figures amount to a dramatic decrease in the amount of on-board fuel: at the expense of roughly the threefold flight time the weight of the fuel can be reduced to at least 1/3 of what is used for *VenusExpress*.

5.6.2.5 Computational details

We are now going to comment on the specific details of the computation for the Earth–Venus transfer trajectory. We are considering the two three-body systems

---

[3] http://sci.esa.int/science-e/www/area/index.cfm?fareaid=64

Sun–Earth–Spacecraft and Sun–Venus–Spacecraft with μ-values of $\mu_{SE} = 3.04041307864 \times 10^{-6}$ and $\mu_{SV} = 2.44770642702 \times 10^{-6}$, respectively.

1. For the construction of the 'gateway set' $\mathcal{O}_1$ we consider the L_1-Lyapunov orbit $\mathcal{L}_1$ associated with the value $C_1 = 3.0005$ of the Jacobi integral in the Sun–Earth system. This value results from experimenting with several different values and eventually bears further optimzation potential. We compute the intersection A_1 of its interior local unstable manifold (i.e., the piece of its local unstable manifold that extends into the interior region) with the section $\Sigma = \{x_1 = 0.98\}$ in the given energy surface $\{C = C_1\}$. Let $\bar{A}_1$ denote the points that are enclosed by the closed curve A_1 in this two-dimensional surface. We set

$$\mathcal{O}_1 = \mathcal{L}_1 \cup (\bar{A}_1 \setminus A_1).$$

Analogoulsy, we compute A_2, $\bar{A}_2$ and $\mathcal{O}_2$ in the Sun–Venus system, using again a value of $C_2 = 3.0005$ for the Jacobi integral. As intersection planes we choose $\Sigma_1 = \Sigma_2 = \{\theta = \frac{\pi}{4}\}$, since this turned out to yield the good compromise between transfer time and Δv.

2. We have been using constant control functions only, employing 800 mN as an upper bound for the maximal thrust. This bound is in accordance with the capabilities of the thrusters that are planned to be used in connection with the *BepiColombo* mission. Here we assumed a mass of 4000 kg for the spacecraft.

3./4. Figure 5.14 shows coverings of the sets $\hat{\mathcal{R}}(\mathcal{O}_1, \tau_1)$ (red) and $\mathcal{R}(\mathcal{O}_2, \tau_2)$ (blue), as well as a covering of their intersection (yellow), projected onto the $(x_1, \dot{x}_1)$-plane. The associated optimal trajectory (i.e., the one with a minimal combined Δv for both
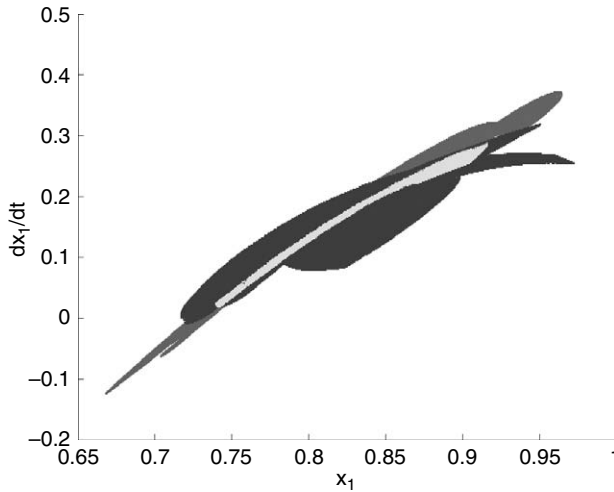

Fig. 5.14. Intersection of two reachable sets in a common intersection plane. Red: reachable set of the gateway set of Earth, blue: reachable set of the gateway set of Venus; yellow: their intersection. Shown is a projection of the covering in three space onto the $(x_1, \dot{x}_1)$-plane (normalized units). (see Color plate 4)
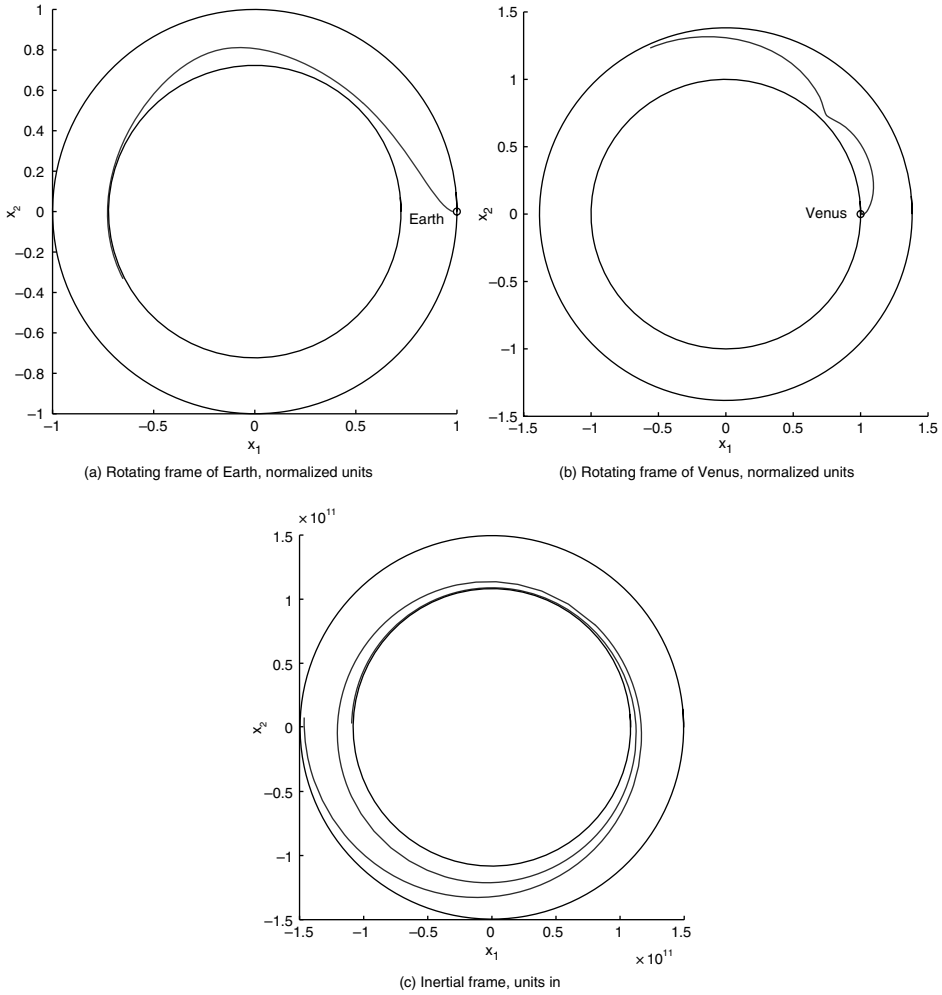
Fig. 5.15. Approximate interplanetary trajectory, joining the gateway sets $\mathcal{O}_1$ (near the Sun–Earth L_1) and $\mathcal{O}_2$ (near the Sun–Venus L_2).

pieces of the trajectory) is shown in Figure 5.15 as seen in the inertial frame as well as in both rotating frames. It requires a (constant) control force of $u_1 = -651$ mN in the first phase (i.e., while travelling from $\mathcal{O}_1$ to Σ_1) and of $u_2 = -96$ mN in the second phase. The corresponding flight times are $|\tau_1| = 0.51$ and $|\tau_2| = 0.92$ years, amounting to a total Δv of approximately 3300 m/s. We note that there still exists a discontinuity in the computed trajectory when switching from the first to the second phase. This is due to the fact that the two pieces of the trajectory are only forced to end in the same box in the intersection plane. However, the radii of the boxes are rather small, namely roughly 10 000 km in position space and ≈ 35 m/s

in the velocity coordinates. This is why we expect the computed trajectory to be a very good initial guess for a standard local solver (e.g., a collocation or multiple shooting approach, see Refs.[15, 16, 37, 39]) for a suitably formulated optimal control problem. In fact, we used the computed trajectory as an initial guess for the solution of a four-body model by a recently developed variational approach to the computation of optimal open loop controls [24].

5.6.2.6 *The complete journey*

In Ref. [11] we complement the above example computation by computing transfer trajectories between the gateway sets $\mathcal{O}_1, \mathcal{O}_2$ and the corresponding planets. We end up with a flight time of roughly 1.8 years and a corresponding Δv of slightly less than 4000 m/s for the complete journey from Earth to Venus.

5.7 Conclusion

Set oriented methods provide a robust framework for the numerical solution of problems in space mission design. Due to the fact that outer approximations of the objects of interest are computed, these methods in particular enable a reliable detection of certain energy efficient trajectories like connecting orbits under the gravitational dynamics or in the low-thrust setting. A particular inherent advantage of this approach is the ability to systematically take into account the propagation of errors as well as the effects of uncertainty—a feature which only has been touched upon in current work and which will be explored in future investigations.

As mentioned above, the numerical effort of our approach crucially depends on the dimension of the object that is being approximated (rather than on the dimension of the underlying phase space). Correspondingly, while it is rather straightforward to treat the case of the full three-dimensional configuration space in Section 5.6, it will be a challenging task to incorporate a fully actuated (i.e., 3D) control, since the dimension of the reachable sets which are being computed will typically be increased.

References

1. Venus express mission definition report. (2001). *European Space Agency, ESA-SCI*, **6**.
2. Abraham, R. and Marsden, J.E. (1978). *Foundations of Mechanics*. Second Edition, Addison-Wesley.
3. Beyn, W.-J. (1990). The numerical computation of connecting orbits in dynamical systems. *IMA Journal of Numerical Analysis*, **9**, pp. 379–405.
4. Beyn, W.-J. (1990). The numerical computation of connecting orbits in dynamical systems. *IMA J. Numer. Anal.*, **10**(3), pp. 379–405.
5. Colonius, F. and Kliemann, W. (2000). The dynamics of control. Systems & Control: Foundations & Applications. Birkhäuser Boston Inc., Boston, MA, 2000.
6. Dellnitz, M., Froyland, G. and Junge, O. (2001). The algorithms behind GAIO-set oriented numerical methods for dynamical systems. In *Ergodic Theory, Analysis, and Efficient Simulation of Dynamical Systems*, pages 145–174, 805–807. Springer, Berlin.

7. Dellnitz, M. and Hohmann, A. (1996). The computation of unstable manifolds using subdivision and continuation. In H.W. Broer, S.A. van Gils, I. Hoveijn, and F. Takens, editors, *Nonlinear Dynamical Systems and Chaos*, pages 449–459. Birkhäuser, *PNLDE* 19.

8. Dellnitz, M. and Hohmann, A. (1997). A subdivision algorithm for the computation of unstable manifolds and global attractors. *Numerische Mathematik*, **75**, pp. 293–317.

9. Dellnitz, M. and Junge, O. (1999). On the approximation of complicated dynamical behavior. *SIAM Journal on Numerical Analysis*, **36**(2), pp. 491–515.

10. Dellnitz, M. and Junge, O. (2002). Set oriented numerical methods for dynamical systems. *In Handbook of Dynamical Systems*, **2**, pp. 221–264. North Holland, Amsterdam.

11. Dellnitz, M., Junge, O., Post, M. and Thiere, B. (2006). On target for Venus—set oriented computation of energy efficient low thrust trajectories. Celestial Mechanics and Dynamical Astronomy, to appear.

12. Dellnitz, M., Junge, O., Post, M. and Thiere, B. (2001). The numerical detection of connecting orbits. *Discrete Contin. Dyn. Syst. Ser. B*, **1**(1), pp. 125–135.

13. Dellnitz, M., Schütze, O. and Hestermeyer, T. (2005). Covering Pareto sets by multilevel subdivision techniques. *JOTA*, **24**(1), pp. 113–136.

14. Dellnitz, M., Schütze, O. and Sertl, St. (2002). Finding zeros by multilevel subdivision techniques. *IMA J. Numer. Anal.*, **22**(2), pp. 167–185.

15. Deuflhard, P. and Bornemann, F. (2002). *Scientific Computing with Ordinary Differential Equations, Texts in Applied Mathematics*, **42**, Springer-Verlag, New York.

16. Deuflhard, P., Pesch, H.-J. and Rentrop, P. (1976). A modified continuation method for the numerical solution of nonlinear two-point boundary value problems by shooting techniques. *Numer. Math.*, **26**(3), pp. 327–343.

17. Doedel, E.J. and Friedman, M.J. (1989). Numerical computation of heteroclinic orbits. *Journal of Computational and Applied Mathematics*, **26**, pp. 155–170.

18. Fabrega, J., Schirmann, T., Schmidt, R. and McCoy, D. (2003). Venus express: The first European mission to Venus. *International Astronautical Congress*, IAC-03-Q.2.06, pp. 1–11.

19. Grüne, L. and Junge, O. (2005). A set oriented approach to optimal feedback stabilization. *Systems Control Lett.*, **54**(2), pp. 169–180.

20. Guckenheimer, J. and Holmes, Ph. (1983). *Nonlinear Oscillations, Dynamical Systems, and Bifurcations of Vector Fields*. Springer.

21. Hairer, E., Nørsett, S.P. and Wanner, G. (1993). *Solving Ordinary Differential Equations. I, Springer Series in Computational Mathematics*, **8**, Springer-Verlag, Berlin, second edition, Nonstiff problems.

22. Hsu, H. (1992). Global analysis by cell mapping. *Int. J. Bif. Chaos*, **2**, pp. 727–771.

23. Junge, O. (1999). *Mengenorientierte Methoden zur numerischen Analyse dynamischer Systeme*. PhD thesis, University of Paderborn.

24. Junge, O., Marsden, J.E. and Ober-Blöbaum, S. (2005). Discrete mechanics and optimal control. *Proceedings of the 16th IFAC World Congress (electronic)*.

25. Junge, O. and Osinga, H.M. (2004). A set oriented approach to global optimal control. *ESAIM Control Optim. Calc. Var.*, **10**(2), pp. 259–270 (electronic).

26. Koon, W.S., Lo, M.W., Marsden, J.E. and Ross, S.D. (2000). Shoot the moon. *AAS/AIAA Astrodynamics Specialist Conference, Florida*, **105**, pp. 1017–1030.

27. Koon, W.S., Lo, M.W., Marsden, J.E. and Ross, S.D. (2002). Constructing a low energy transfer between jovian moons. *Contemporary Mathematics*, **292**, pp. 129–145.

28. Kreuzer, E. (1987). *Numerische Untersuchung nichtlinearer dynamischer Systeme*. Springer.

29. Lo, M.W., Williams, B.G., Bollman, W.E., Han, D., Hahn, Y., Bell, J.L., Hirst, E.A., Corwin, R.A., Hong, P.E., Howell, K.C., Barden, B. and Wilson, R. (2001). Genesis mission design. *Journal of Astronautical Sciences*, **49**, pp. 169–184.

30. McGehee, R.P. (1969). *Some homoclinic orbits for the restricted 3-body problem*. PhD thesis, University of Wisconsin.

31. Meyer, K.R. and Hall, R. (1992). *Hamiltonian Mechanics and the n-body Problem*. Springer-Verlag, Applied Mathematical Sciences.

32. Lo, M.W., Williams, B.G., Bollman, W.E., Han, D.S., Hahn, Y.S., Bell, J.L., Hirst, E.A., Corwin, R.A., Hong, P.E., Howell, K.C., Barden, B. and Wilson, R. (2001). Genesis mission design. *J. Astron. Sci.*, **49**, pp. 169–184.

33. Schütze, O. (2003). A new data structure for the nondominance problem in multi-objective optimization. In *Evolutionary Multi-Criterion Optimization*, (Carlos M. Fonseca, Peter J. Fleming, Eckart Zitzler, Kalyanmoy Deb, and Lothar Thiele, eds.), *Lecture Notes in Computer Science*, **2632**, pp. 509–518. Springer.

34. Schütze, O., Mostaghim, S., Dellnitz, M. and Teich, J. (2003). Covering Pareto sets by multilevel evolutionary subdivision techniques. In *Evolutionary Multi-Criterion Optimization*, (Carlos M. Fonseca, Peter J. Fleming, Eckart Zitzler, Kalyanmoy Deb, and Lothar Thiele, eds.), *Lecture Notes in Computer Science*, **2632**, pp. 118–132. Springer.

35. Sertl, S. and Dellnitz, M. (2006). Global optimization using a dynamical systems approach. *J. Glob. Opt.*, in press.

36. Spreuer, H. and Adams, E. (1993). On the existence and the verified determination of homoclinic and heteroclinic orbits of the origin for the Lorenz equations. In *Validation Numerics*, (R. Albrecht, G. Alefeld, and H.J. Stetter, eds.), pp. 233–246. Springer.

37. Stoer, J. and Bulirsch, R. (2002). *Introduction to numerical analysis*, **12**, Springer-Verlag, New York, 2002.

38. Szebehely, V. (1967). *Theory of Orbits—The Restricted Problem of Three Bodies*. Academic Press.

39. von Stryk, O. (1993). Numerical solution of optimal control problems by direct collocation. In *Optimal Control—Calculus of Variations, Optimal Control Theory and Numerical Methods* (R. Bulirsch, A. Miele, J. Stoer, and K.-H. Well, ed.), *Internat. Ser. Numer. Math.*, **111**, pp. 129–143. Birkhäuser, Basel.
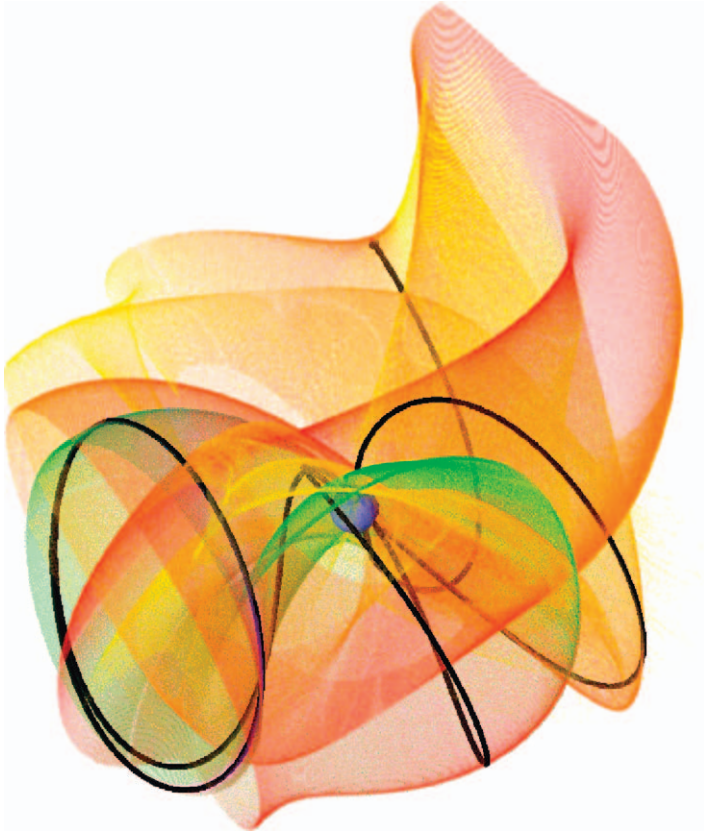
Color plate 1. Covering of part of the global unstable manifold of an unstable periodic orbit in the circular restricted three-body problem (projection onto configuration space). The blue body depicts the Earth, the black trajectory is a sample orbit which leaves the periodic orbit in the direction of the Earth. The coloring indicates the temporal distance from the periodic orbit. (see Fig. 5.5)
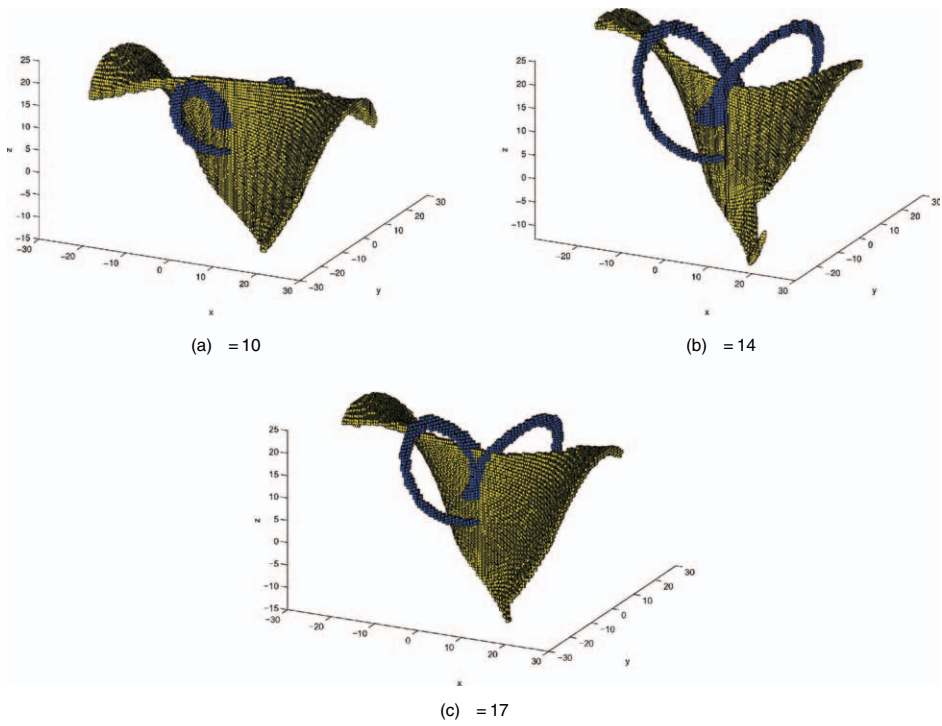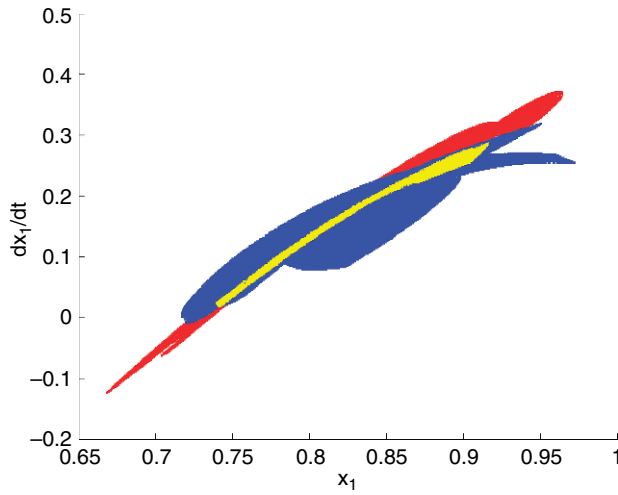
(c) $k = 15$

(b) $k = 21$
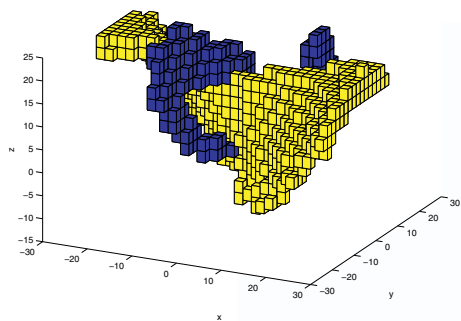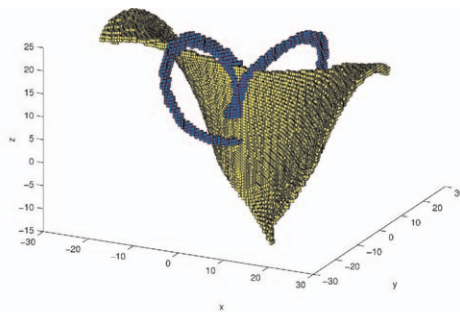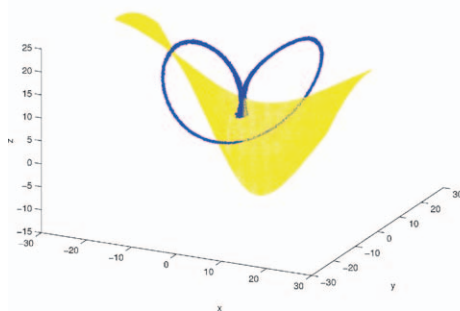
(c) $k = 27$

Color plate 2. Lorenz system: The coverings $\mathcal{U}_{(k)}(14)$ (blue) and $\mathcal{S}_{(k)}(14)$ (yellow) for different k. (see Fig. 5.11)

(a) $\rho = 10$

(b) $\rho = 14$

(c) $\rho = 17$

Color plate 3. Lorenz system: The coverings $\mathcal{U}^{(21)}(\rho)$ (blue) and $\mathcal{S}^{(21)}(\rho)$ (yellow) in dependence of ρ. (see Fig. 5.12)

Color plate 4. Intersection of two reachable sets in a common intersection plane. Red: reachable set of the gateway set of Earth, blue: reachable set of the gateway set of Venus; yellow: their intersection. Shown is a projection of the covering in three space onto the $(x_1, \dot{x}_1)$-plane (normalized units). (see Fig. 5.14)